HFVS: An Arbitrary High Order Flux Vector Splitting Method *

Yibing Chen , Song Jiang and Na Liu

Institute of Applied Physics and Computational Mathematics,
P.O. Box 8009, Beijing 100088, P.R. China

E-mail: chen_yibing@iapcm.ac.cn, jiang@iapcm.ac.cn, liu_na@iapcm.ac.cn

Abstract

In this paper, a new scheme of arbitrary high order accuracy in both space and time is proposed to solve hyperbolic conservative laws. Based on the idea of flux vector splitting(FVS) scheme, we split all the space and time derivatives in the Taylor expansion of the numerical flux into two parts: one part with positive eigenvalues, another part with negative eigenvalues. According to a Lax-Wendroff procedure, all the time derivatives are then replaced by space derivatives. And the space derivatives is calculated by WENO reconstruction polynomial. One of the most important advantages of this new scheme is easy to implement.In addition, it should be pointed out, the procedure of calculating the space and time derivatives in numerical flux can be used as a building block to extend the current first order schemes to very high order accuracy in both space and time. Numerous numerical tests for linear and nonlinear hyperbolic conservative laws demonstrate that new scheme is robust and can be high order accuracy in both space and time.

Keywords. Flux vector splitting scheme, arbitrary high order accuracy , space and time, hyperbolic conservative laws

1 Introduction

In the recent years, numerical schemes of high order accuracy for hyperbolic conservative laws have attracted much attention. In the 1980s, thanks to the efforts of Harten [7],

*Supported by NSFC(Grant No. 11101047) .

Van Leer [18] and Roe [12] et al. (only a partial list is given here), schemes of second order accuracy tend to maturity. Later, ENO/WENO schemes show a possibility to construct the schemes of arbitrary high order accuracy in space [6, 8]. And since the end of the 1990s, designing schemes of high order accuracy (greater than second order accuracy) becomes one of the most important issues in CFD. In practical simulations, ENO/WENO schemes usually couple with the multi-stage Runge-Kutta method for time evolution. In implementation , the third order TVD Runge-Kutta method is often used [1]. This is because higher than third order Runge-Kutta methods will become complicate. For example, fourth order TVD Runge-Kutta method needs to save all the variables in intermediate stages, which will definitely introduce more computational complexity. What's worse, higher than fourth order Runge-Kutta method will meet the so-called Butcher barrier[3], which the number of stages will greater than the order of accuracy (e.g., fifth order Runge-Kutta method need six stages). But third order Runge-Kutta method will also lead to accuracy barrier, for example, the fifth order WENO scheme couples with the third order TVD Runge-Kutta method can only achieve third order accuracy [15]. To obtain ideal convergence rate, one has to reduce the CFL condition number, which will increase the computational costs.

At the first decade of this century, many researchers made great efforts to avoid the above drawback. The first milestone may belong to the ADER (Arbitrary DERivative in space and time) scheme, which is a Godunov approach based scheme of arbitrary high order accuracy in both space and time [15]. The idea of ADER scheme can go back to the GRP scheme [2], which solves the generalized Riemann problem with piecewise linear initial values instead of the conventional Riemann problem with piecewise constant initial values. The GRP scheme is sophisticated, but may become quite complicated in the case of higher than third order accuracy. By introducing a linearization technique, the ADER scheme transfers a generalized Riemann problem into a conventional Riemann problem coupled with a series of linear hyperbolic problems. This transfer process much simplifies the computational process of the original GRP scheme and makes it possible to construct schemes of arbitrary high order accuracy both in space and time.

The ADER scheme can be divided into two camps, the one is state-expansion [15], another one is flux-expansion [17]. The former can not be integrated explicitly in time, so a Gaussian quadrature is necessary for high order accuracy. On the other hand, the latter can be integrated exactly in time, the time derivatives of the numerical flux, however, have to be given explicitly, and it could be very tedious when the formulation of the numerical flux is complex. If one chooses a nonlinear Riemann problem solver such as HLLC, it is not trivial to deduce the formulation of high order derivative terms. That is why the flux expansion version ADER is more difficult to implement than the

state expansion one.

Besides ADER scheme, HGKS (high-order accurate gas-kinetic scheme) is another important scheme of high order accuracy [9, 10], which is a gas kinetic scheme. HGKS is based on the Boltzmann equation, then the time derivatives in the Taylor expansion of the particle distribution function can be replaced by space derivatives directly. Comparing to the ADER scheme, the numerical flux in HGKS can be obtained without a linearization process. HGKS can be also integrated exactly in time and made to be of arbitrary high order accuracy both in space and time. We should point out, however, that the formulation of HGKS may also become quite complex in the high order accuracy case. Although the recursive techniques simplify the procedure of deduction in the high order HGKS, the computational costs can not be reduced. In fact, the computational costs in CPU time for HGKS may greater than those for WENO with Godunov Riemann problem solvers, see [11]. Another drawback for HGKS is that there are some spurious velocity and pressure oscillations near the contact discontinuous when HGKS is used to solve the Euler equations. This phenomenon is found and carefully analyzed by the authors in [4]. A remedy for the GKS coupled with the Runge-Kutta method is also provided in their articles [4, 5]. However, how to construct an oscillation-free HGKS (greater than second order accuracy) is still unsolved.

In recent fifteen years, the ADER scheme and HGKS have provided a new approach to construct schemes of high order accuracy. In this article, we present a new simple version to construct a high order scheme and propose thus a numerical scheme of arbitrary high order accuracy in both space and time. Different from the ADER scheme and HGKS, our new scheme is based on the flux vector splitting method, and is much easier to implement and robust. We call the new scheme HFVS (arbitrary high order flux vector splitting scheme). We shall give a number of numerical tests to demonstrate the efficiency and accuracy of HFVS.

This paper is organized as follows. In Section 2, we present the framework of numerical schemes of arbitrary high order accuracy in both space and time, while in Section 3 we give the construction of our new scheme HFVS in details. In Section 4 we test HFVS in accuracy by a number of numerical examples of linear and nonlinear conservative laws in 1D and 2D, and compare the numerical results computed by HFVS and those by WENO in both accuracy and computational costs. Finally, we draw the conclusions.

2 Framework of numerical schemes of high order accuracy in both space and time

As mentioned in the previous section, the ADER scheme is a Godunov scheme based approach, while HGKS is a Boltzmann equation based approach. In our opinion, the flux-expansion version of the ADER scheme and HGKS can be classified in a unified framework of high order schemes in both space and time. In fact, Toro's original article[17] implies the possibility. Here we want to make the framework more clearly.

Let us start with a one-dimensional hyperbolic system of conservation laws in the form:

$$\frac{\partial \vec{W}}{\partial t} + \frac{\partial \vec{F}(\vec{W})}{\partial x} = 0. \tag{2.1}$$

To simplify the presentation, we consider here the 1D Euler equations of compressible flows in this section, although both the ADER scheme and HGKS are constructed for general hyperbolic conservation laws. For the the 1D Euler equations, $\vec{W}$ and F in (2.1) are given by

$$\begin{aligned} \vec{W} &= \big(\rho, \rho U, \rho E\big)^T, \\ \vec{F}(\vec{W}) &= \big(\rho U, \rho U^2 + P, \rho E U + P U\big)^T, \end{aligned} \tag{2.2}$$

where, ρ, U, E, P are the density, fluid velocity, specific total energy and pressure, respectively. The system can be closed by adding the equations of state (perfect gases):

$$P = (\gamma - 1)\rho\Big(E - \frac{1}{2}U^2\Big).$$

Integrating (2.1) over a space-time computational cell $[x_{j-\frac{1}{2}}, x_{j+\frac{1}{2}}] \times [t^n, t^{n+1}]$, we have

$$\int_{t^n}^{t^{n+1}} \int_{x_{j-\frac{1}{2}}}^{x_{j+\frac{1}{2}}} \left(\frac{\partial \vec{W}}{\partial t} + \frac{\partial \vec{F}(\vec{W})}{\partial x} \right) dx dt = 0. \tag{2.3}$$

Denote $\Delta x = [x_{j-\frac{1}{2}}, x_{j+\frac{1}{2}}]$ and $\Delta t = [t^n, t^{n+1}]$, we approximate (2.3) by the classical finite volume method (FVM)

$$\vec{W}_j^{\,n+1} = \vec{W}_j^{\,n} - \frac{1}{\Delta x} \int_{t^n}^{t^{n+1}} \Big(\vec{F}_{j+\frac{1}{2}} - \vec{F}_{j-\frac{1}{2}} \Big) dt, \tag{2.4}$$

where $\vec{W}_j^{\,n}$ is the cell average of $\vec{W}(x, t^n)$ ($x \in [x_{j-\frac{1}{2}}, x_{j+\frac{1}{2}}]$) and $\vec{F}_{j+\frac{1}{2}}$ is the numerical flux. To make the scheme (2.4) high order accuracy, the key point is to suitably construct the numerical flux which should be in high order accuracy.

The procedure to construct a numerical scheme with high order accuracy in both space and time can be divided into three steps.

Step I. Construct $\vec{F}_{j+\frac{1}{2}}(0^+)$ by the Taylor expansion of the numerical flux as follows.

$$\vec{F}_{j+\frac{1}{2}}(\tau) = \vec{F}_{j+\frac{1}{2}}(0^+) + \sum_{k=1}^{N} \frac{\partial^k}{\partial t^k} \vec{F}_{j+\frac{1}{2}}(0^+) \frac{\tau^k}{k!}. \tag{2.5}$$

Step II. Replace the time derivatives by spatial derivatives.

Step III. Calculate the space derivatives by certain reconstruction techniques.

In the above procedure, a WENO reconstruction technique is used in Step III for the ADER scheme and HGKS, while very different techniques are employed in Steps I and II, and described in the following.

2.1 The ADER scheme

In the ADER scheme, an approximate Riemann solver such as HLLC is used in Step II:

$$\vec{F}_{j+\frac{1}{2}}(0^+) = \begin{cases} \vec{F}_j, & if\ 0 \le\ S_j, \\ \vec{F}_j + S_j \left(\vec{W}_j^{\,*} - \vec{W}_j \right), & if\ S_j \le 0 \le\ S^*, \\ \vec{F}_{j+1} + S_{j+1} \left(\vec{W}_j^{\,*} - \vec{W}_j \right), & if\ S^* \le 0 \le\ S_{j+1}, \\ \vec{F}_{j+1}, & if\ 0\ \ge S_j, \end{cases}$$

where

$$\vec{W}_k^{\,*} = \rho_k \left(\frac{S_k - U_k}{S_k - U^*} \right) \begin{bmatrix} 1 \\ S^* \\ E_k + (S^* - U_k) \left(S^* + \frac{P_k}{\rho_k (S_k - U_k)} \right) \end{bmatrix}, k = j\ or\ j+1$$

The wave speed of S_j, $S_j + 1$ and S^* can have many choices, see [16].

Then, the time derivatives of numerical flux in (2.5) can be given analytically, for example, as follows.

$$\begin{aligned} \frac{\partial \vec{F}}{\partial t} &= \left[(\rho U)_t, (\rho U)_t U + (\rho U) U_t + P_t, U_t (\rho E + P) + U (\rho E + P)_t \right]^T, \\ \frac{\partial^2 \vec{F}}{\partial t^2} &= \Big[(\rho U)_{tt}, (\rho U)_{tt} U + 2(\rho U)_t U_t + (\rho U) U_{tt} + P_{tt}, U_{tt} (\rho E + P) \\ &\quad + 2 U_t (\rho E + P)_t + U (\rho E + P)_{tt} \Big]^T. \end{aligned}$$

According to the construction procedure of the Lax-Wendroff scheme, the time derivatives in the above formulations can be replace by the spatial derivatives.

Remark 1. The procedure can be carried out for any given order. However, it is easy to see that these formulations may become very complicate in the case of very high order accuracy , which will increase the complexity in implementation.

2.2 HGKS

Different from the ADER scheme, HGKS is based on the Boltzmann-type equation, such as the BGK model:

$$f_t + uf_x = \frac{g-f}{\tau},$$

where f is the particle velocity distribution function and g is corresponding equilibrium distribution. Both f and g are functions of space x, time t, the particle velocity u, and the internal variables $\vec{\xi} = (\xi_1, \xi_2, \cdots, \xi_K)$, which has K degrees of freedom.

The relationship between the numerical flux and the particle distribution function is

$$\vec{F}_{j+\frac{1}{2}}(\tau) = \int u\Psi f_{j+\frac{1}{2}}(\tau) d\Xi.$$

Here Ψ is the moment vector

$$\Psi = (1, u, \frac{1}{2}(u^2 + \vec{\xi}^2))^T,$$

and the internal variable $\vec{\xi^2}$ is equal to $\vec{\xi^2} = \xi_1^2 + \xi_2^2 + \cdots + \xi_K^2$.

Hence, the time derivatives of numerical flux can be calculated by

$$\frac{\partial^k \vec{F}_{j+\frac{1}{2}}}{\partial t^k} = \int u\Psi \frac{\partial^k f_{j+\frac{1}{2}}}{\partial t^k} d\Xi.$$

In view of the BGK model, the time derivatives can be evaluated directly, for example,

$$\begin{aligned}
f_{j+\frac{1}{2}}(0^+) &= (1-\tau(a^l u + A^l))H(u)g^l + (1-\tau(a^r u + A^r))(1-H(u))g^r, \\
\frac{\partial}{\partial t} f_{j+\frac{1}{2}}(0^+) &= \frac{1}{\tau}g_0 - \tau(a^2+b)u^2 g_0 - \tau(A^2+B')g_0 - 2\tau(C+aA)ug_0 \\
&\quad + [-\frac{1}{\tau} + A^l + \tau(C^l + a^l A^l)u + \tau((a^l)^2 + b^l)u^2]H(u)g^l \\
&\quad + [-\frac{1}{\tau} + A^r + \tau(C^r + a^r A^r)u + \tau((a^r)^2 + b^r)u^2](1-H(u))g^r, \\
\frac{\partial^2}{\partial t^2} f_{j+\frac{1}{2}}(0^+) &= -\frac{1}{\tau^2}g_0 - \frac{1}{\tau}aug_0 + \frac{1}{\tau}Ag_0 + (a^2+b)u^2 g_0 + (A^2+B')g_0 + 2(C+aA)ug_0 \\
&\quad + [\frac{1}{\tau^2} - \frac{1}{\tau}(a^l u + A^l) + \frac{2}{\tau}a^l u - 2(C^l + a^l A^l)u - ((a^l)^2 + b^l)u^2]H(u)g^l \\
&\quad + [\frac{1}{\tau^2} - \frac{1}{\tau}(a^r u + A^r) + \frac{2}{\tau}a^r u - 2(C^r + a^r A^r)u - ((a^r)^2 + b^r)u^2](1-H(u))g^r.
\end{aligned}$$

Here g_0 is the Maxwellian distribution at the cell interface $x_{j+\frac{1}{2}}$, g^l and g^r are the left and right limits of the Maxwellian distribution at the cell interface, repsectively. $a, b, A, \cdots$

are related to the space and time derivatives of the the Maxwellian distribution, see [10] for the detailed definition.

Remark 2. Theoretically, HGKS can achieve arbitrary high order accuracy. However, due to its complexity in the expression, only third and fourth order schemes are often used in simulations[9, 10].

In the following section, we want to present a simpler high order scheme, which is different from the ADER scheme and HGKS.

3 HFVS: Arbitrary high order flux vector splitting scheme

From the last section, we can see that the complexity of the flux expansion version of the ADER scheme and HGKS actually comes from the procedure of evaluating the time derivatives of the numerical fluxes. So, if one can find a numerical flux, the time derivatives of which can be calculated very easily, then the complexity of the associated numerical scheme can be largely reduced. This motivates us to construct our scheme.

As is well-known, in comparison with the traditional Godunov scheme, flux vector splitting (FVS) schemes are simpler in construction and coding. Thus, we try to use the FVS approach, instead of the Godunov approach used in the ADER scheme. Our proposed scheme is constructed in the same framework as in Section 2, and also consists of three phases: constructing spatial derivatives, leading terms and time derivatives.

3.1 Spatial derivatives

In order to diminish possible spurious oscillations, we should use conservative reconstruction techniques such as ENO/WENO to evaluate spatial derivatives.

Suppose that a smooth function over a cell should be reconstructed, which is of the form:

$$\vec{W}(x) = \vec{W}_j + \sum_{k=1}^{N} \frac{\partial^k \vec{W}}{\partial x^k} \phi_k(x), \qquad x \in [x_{j-\frac{1}{2}}, x_{j+\frac{1}{2}}], \tag{3.6}$$

where $\vec{W}_j$ is the cell known averaged value of $\vec{W}$ over cell j, $\partial^k \vec{W}/\partial x^k$ $(k = 1, \cdots, N)$ are the unknowns to be determined, and

$$\varphi_1 = \Big(\frac{x - x_j}{\Delta x}\Big), \quad \varphi_2 = \frac{1}{2}\Big[\Big(\frac{x - x_j}{\Delta x}\Big)^2 - \frac{1}{12}\Big], \quad \varphi_3 = \frac{1}{6}\Big(\frac{x - x_j}{\Delta x}\Big)^3,$$
$$\varphi_4 = \frac{1}{24}\Big[\Big(\frac{x - x_j}{\Delta x}\Big)^4 - \frac{1}{80}\Big], \quad \cdots$$

In general, we can always obtain two values on cell interfaces by the ENO/WENO reconstruction techniques, i.e., $\vec{W}_{j\pm\frac{1}{2}}$. Thus, we immediately obtain two linear **algebraic** equations:

$$\begin{cases} \vec{W}(x_{j+\frac{1}{2}}) = \vec{W}_{j+\frac{1}{2}}, \\ \vec{W}(x_{j-\frac{1}{2}}) = \vec{W}_{j-\frac{1}{2}}. \end{cases} \tag{3.7}$$

In this case , these formulations also implies

$$\frac{1}{\Delta x}\int_{I_j} \vec{W}(x)dx = \vec{W}_j. \tag{3.8}$$

When the dimension $N = 1$, the above system is uniquely solvable.

For $N > 1$, supplementary information should be added in order to have a solution of the system (3.7). A simple way of giving the supplementary information is to employ the cell averaged values. For example, for $N = 2$ we use

$$\frac{1}{\Delta x}\int_{I_j} \vec{W}(x)dx = \vec{W}_j. \tag{3.9}$$

Coupling (3.9) with (3.7), we obtain a system of three independent linear equations for the three unknowns, which is uniquely solvable.

Similarly, for $N = 4$ we use

$$\frac{1}{\Delta x}\int_{I_l} \vec{W}(x)dx = \vec{W}_l, \qquad l = j-1, j, j+1,$$

instead of (3.9). Obviously, this choice is suitable for the case of arbitrary high order accuracy.

In fact, the spatial derivatives can be given explicitly, see below.

Second order.

$$\left(\frac{\partial \vec{W}}{\partial x}\right)_j = \vec{W}_{j+\frac{1}{2}} - \vec{W}_{j-\frac{1}{2}} \tag{3.10}$$

Third order.

$$\begin{aligned} \left(\frac{\partial \vec{W}}{\partial x}\right)_j &= \vec{W}_{j+\frac{1}{2}} - \vec{W}_{j-1} \\ \left(\frac{\partial^2 \vec{W}}{\partial x^2}\right)_j &= 3(-2\vec{W}_{j+1} + \vec{W}_{j+\frac{1}{2}} + \vec{W}_{j-\frac{1}{2}}) \end{aligned} \tag{3.11}$$

Fifth order.

$$\begin{aligned}
\left(\frac{\partial \vec{W}}{\partial x}\right)_j &= \tfrac{1}{8}(\vec{W}_{j-1} - \vec{W}_j - 10\vec{W}_{j-\frac{1}{2}} + 10\vec{W}_{j+\frac{1}{2}}) \\
\left(\frac{\partial^2 \vec{W}}{\partial x^2}\right)_j &= \tfrac{1}{8}(-\vec{W}_{j-1} - 50\vec{W}_j - \vec{W}_{j+1} + 30\vec{W}_{j+\frac{1}{2}} + 30\vec{W}_{j-\frac{1}{2}}) \\
\left(\frac{\partial^3 \vec{W}}{\partial x^3}\right)_j &= \tfrac{1}{2}(-\vec{W}_{j-1} + \vec{W}_{j+1} - 2\vec{W}_{j+\frac{1}{2}} + 2\vec{W}_{j-\frac{1}{2}}) \\
\left(\frac{\partial^4 \vec{W}}{\partial x^4}\right)_j &= \tfrac{5}{12}(\vec{W}_{j-1} + 10\vec{W}_j + \vec{W}_{j+1} - 6\vec{W}_{j+\frac{1}{2}} - 6\vec{W}_{j-\frac{1}{2}})
\end{aligned} \tag{3.12}$$

3.2 Leading terms

Following the idea of FVS, the flux in a computational cell can be decomposed into two parts:

$$\vec{F}_j = \vec{F}_j^{+} + \vec{F}_{j+1}^{-}.$$

Thus the numerical flux on a cell edge consists of two parts:

$$\vec{F}_{j+\frac{1}{2}}(0^+) = \vec{F}_j^{+}(0^+) + \vec{F}_{j+1}^{-}(0^+). \tag{3.13}$$

By a first-order Steger-Warming scheme [14], we have

$$\vec{F}^{\pm}(\vec{W}) = A^{\pm}\vec{W}, \tag{3.14}$$

where $A^{\pm} = L\Lambda^{\pm}R$, L and R are the left and right eigenvectors respectively, $\Lambda^{\pm}$ are the diagonal matrices of positive resp. negative eigenvalues. On the other hand, we also have

$$\vec{F}(\vec{W}) = A\vec{W}, \tag{3.15}$$

where $A = L\Lambda R$ is the Jacobian matrix, $\Lambda = \Lambda^+ + \Lambda^-$ is the diagonal matrix of eigenvalues.

3.3 Time derivatives

By virtue of (3.14), (2.1) and (3.15), omitting the subscripts, we obtain the time derivatives of two parts in (3.13):

$$\frac{\partial}{\partial t}\vec{F}^{\pm} = A^{\pm}\frac{\partial}{\partial t}\vec{W} = A^{\pm}\left(-A\frac{\partial}{\partial x}\vec{W}\right).????$$

Generally, we have

$$\frac{\partial^k}{\partial t^k}\vec{F}^{\pm} = \frac{\partial^{k-1}}{\partial t^{k-1}}\frac{\partial}{\partial t}\vec{F}^{\pm} = \frac{\partial^{k-1}}{\partial t^{k-1}}\left(A^{\pm}\left(-A\frac{\partial}{\partial x}\vec{W}\right)\right) = A^{\pm}(-A)^k\frac{\partial^k}{\partial x^k}\vec{W}. \tag{3.16}$$

Hence, we can easily get the numerical flux (in high order accuracy) as follows.

$$\vec{F}_{j+\frac{1}{2}}(\tau) = \vec{F}_{j+\frac{1}{2}}(0^+) + A^{\pm}\sum_{k=1}^{N}(-A)^k\frac{\partial^k\vec{W}}{\partial x^k}\frac{\tau^k}{k!}, \tag{3.17}$$

where the spatial derivatives $\partial^k\vec{W}/\partial x^k$ $(k = 1, \cdots, N)$ are given in 3.10-3.12.

Remark 3. From the above construction procedure, we can see the new scheme HFVS has two advantages. Firstly , it is obviously simpler than the original ADER and HGKS. The main reason is: the high order time derivatives can be expressed by a explicit and compact formulation of high order space derivatives, which makes the computational procedures clear and easy to implement. In addition, HFVS evidently used less computational costs than ADER and HGKS. This is also attributed to the simpler procedure to compute the high derivative terms.

Remark 4. Although the Steger-Warming scheme is used as the leading term in the construction of our scheme, we should point out that the leading term in (3.17) can be arbitrary Riemann solver, such as the HLLC and BGK solvers. This means the latter terms can be used as a building block to extend the current FVS scheme to high order accuracy in both space and time.

4 Numerical tests

In this section, we present the numerical experiment results for linear and nonlinear hyperbolic conservative laws in 1D and 2D. We call our new scheme the HFVS (arbitrary High order Flux Vector Splitting) scheme. The abbreviations HFVS2, HFVS3 and HFVS5 mean the second-, third- and fifth-order HFVS schemes, respectively. owing to the simplicity, all numerical schemes only use conservative variables ENO/WENO reconstruction techniques. And we will find they work well enough in most of the cases below.

4.1 Linear hyperbolic problems

In this subsection, we want to examine the accuracy of the new schemes by solving some linear hyperbolic problems.

Example 1. Accuracy test.

We consider the following linear convection equation

$$\frac{\partial w}{\partial t} + \frac{\partial w}{\partial x} = 0$$

with initial data

$$w_0(x) = \sin(2\pi x).$$

We take the unit interval $(0, 1)$ as the computational region and prescribe suitable boundary conditions (inflow boundary condition).

Table I shows the errors and accuracy for different schemes using a same CFL number 0.95 at a computational time $t = 1.0$. We can observe that all HFVS schemes can reach their designed order accuracy.

Table 1: Errors and accuracy for WENO and HFVS

METHOD	N	L_1ERROR	ORDER	L_2ERROR	ORDER	$L_\infty ERROR$	ORDER
HFVS2	20	0.28		0.28		0.31	
	40	0.57E-01	2.34	0.65E-01	2.15	0.92E-01	1.76
	80	0.12E-01	2.21	0.13E-01	2.25	0.19E-01	2.24
	160	0.29E-02	2.07	0.32E-02	2.08	0.46E-02	2.08
	320	0.73E-03	2.01	0.81E-03	2.01	0.11E-02	2.01
	640	0.18E-03	2.01	0.20E-03	2.01	0.28E-03	2.01
HFVS3	20	2.32E-01		2.54E-01		3.35E-01	
	40	3.92E-02	2.56	4.38E-02	2.53	6.14E-02	2.44
	80	5.26E-03	2.89	5.86E-03	2.90	8.27E-03	2.89
	160	6.62E-04	2.99	7.36E-04	2.99	1.04E-03	2.99
	320	8.13E-05	3.02	9.03E-05	3.02	1.28E-04	3.02
	640	1.02E-05	2.99	1.13E-05	2.99	1.60E-05	3.00
HFVS5	20	1.02E-01		1.17E-01		1.59E-01	
	40	4.75E-03	4.42	5.35E-03	4.45	7.51E-03	4.40
	80	1.62E-04	4.87	1.81E-04	4.88	2.55E-04	4.88
	160	5.14E-06	4.97	5.71E-06	4.98	8.08E-06	4.97
	320	1.58E-07	5.02	1.75E-07	5.02	2.48E-07	5.02
	640	4.93E-09	5.00	5.48E-09	4.99	7.75E-09	5.00

4.2 Nonlinear hyperbolic problem

In this section, we continue to present the numerical results of 1D and 2D Euler equations of compressible flows.

4.2.1 1D Euler equations

The Governing equations of 1D Euler equations can see 2.2. In this section, $\gamma = 1.4$,and all numerical schemes use an optimal CFL number 0.95.

Example 2. Shu-Osher shock turbulence interaction problem[13].

the computational domain is $[-1, 1]$, and the initial condition is

$$(\rho, u, P) = \begin{cases} (3.857143, 2.629369, 10.333333), x < -0.8 \\ (1 + 0.2 \sin 5\pi x, 0.0, 1.0) \qquad , x > -0.8 \end{cases}$$

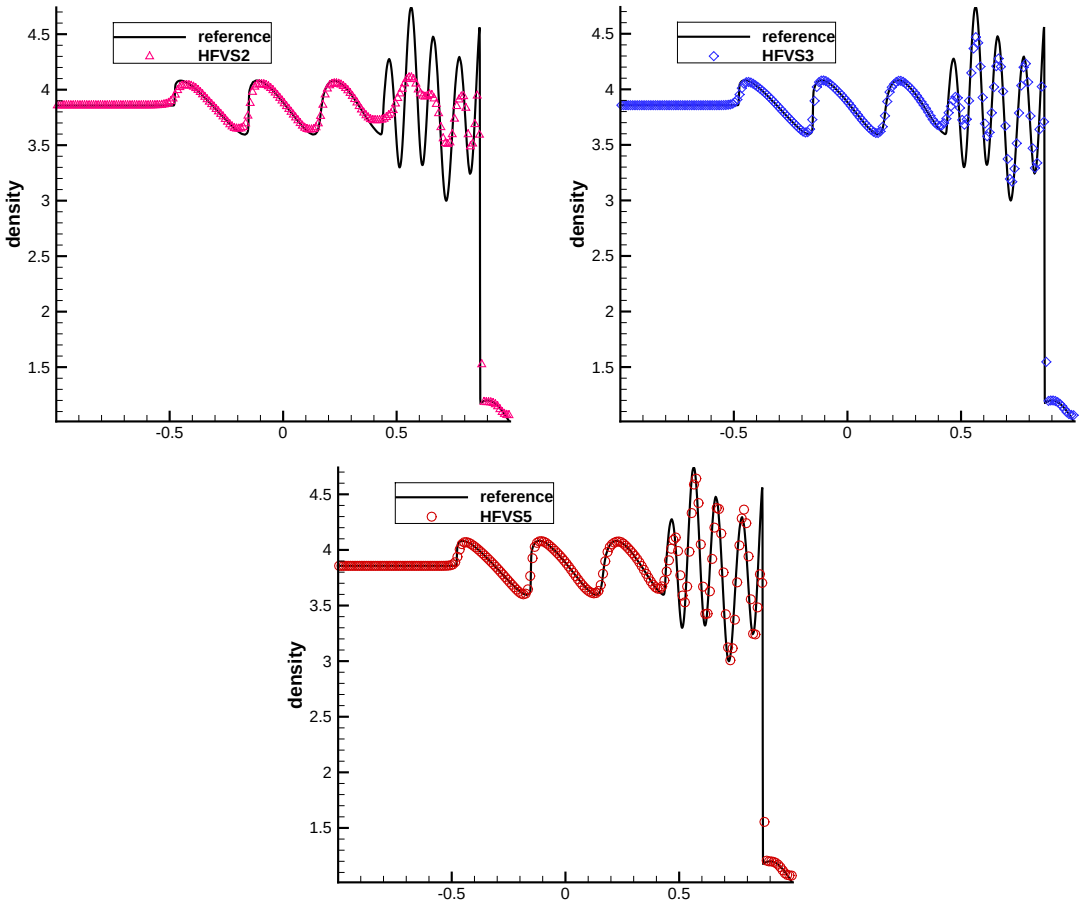

Figure 1: Example 2. density profiles for different schemes.

Figs.1 and Figs.2 shows the density , pressure and internal profiles computed by different schemes $t = 0.47$ with mesh of 200 cells. And a reference solution is computed by the third order WENO scheme on a fine mesh with 2000 cells. We can observe that all schemes can resolve the complex solution of the governing equation. In addition, HFVS2 introduces over diffusion, and HFVS3 improves the resolution, while HFVS5 gives a sharp profile. This also demonstrates the advantages of high order scheme.

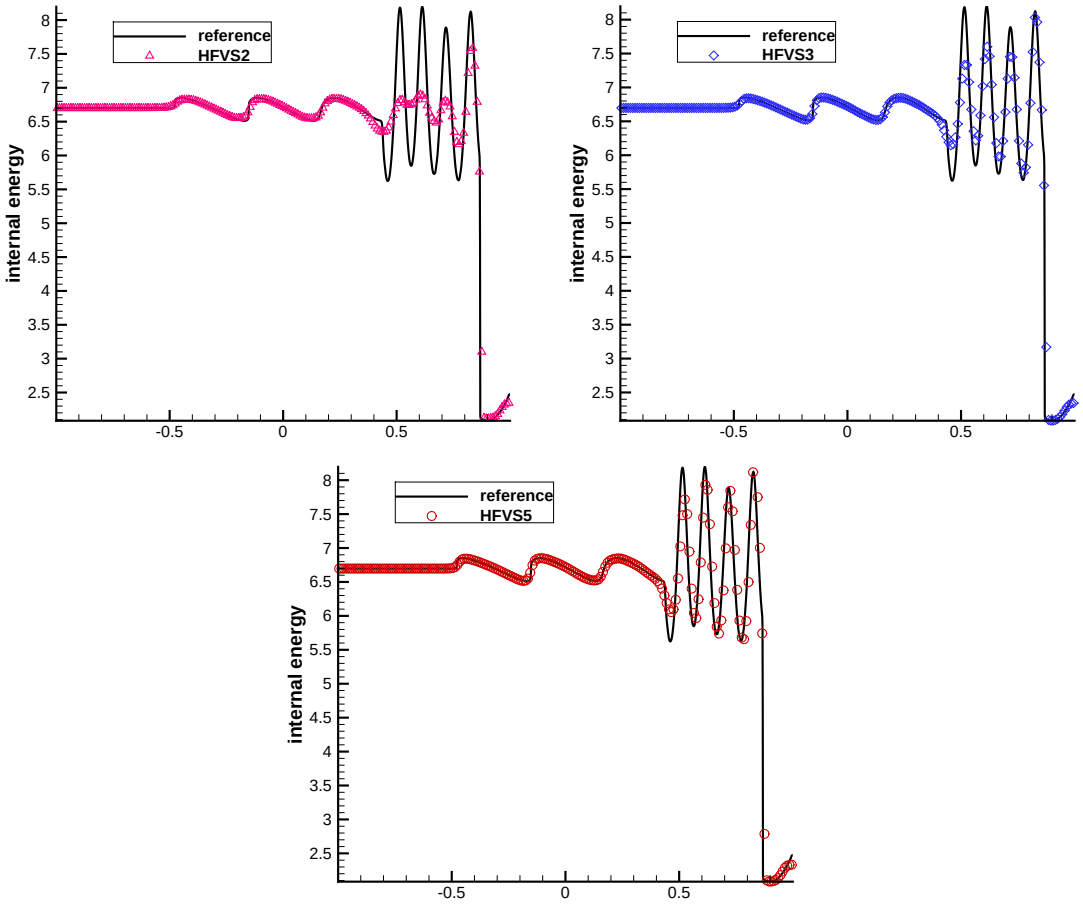

Figure 2: Example 2. internal energy profiles for different schemes.

Example 3 Woodward-Colella blast wave problem[19]. The computational domain is $[0, 1]$ with reflected boundary conditions on both sides, and the initial condition is

$$(\rho, U, P) = \begin{cases} (1, 0, 1000), 0 \leq x \leq 0.1 \\ (1, 0, 0.01), 0.1 \leq x \leq 0.9 \\ (1, 0, 100), 0.9 \leq x \leq 1.0 \end{cases}$$

This is problem with high ratio of pressure and the solution includes strong shock waves, contact discontinuities, rarefaction waves and their interactions. So it is a very challenging problem for high order schemes.

Fig.3 and Fig.4 shows the numerical results at computational time $t = 0.038$ with mesh of 800 cells. The reference solution is computed by third order WENO on 10000 cells. All HFVS schemes can resolve all the waves of the flow. As the previous test problem, HFVS2 gives poor solution, HFVS3 greatly improve the resolution, and HFVS5

can give a sharp picture. The numerical results can demonstrate the robustness and accuracy of HFVS.

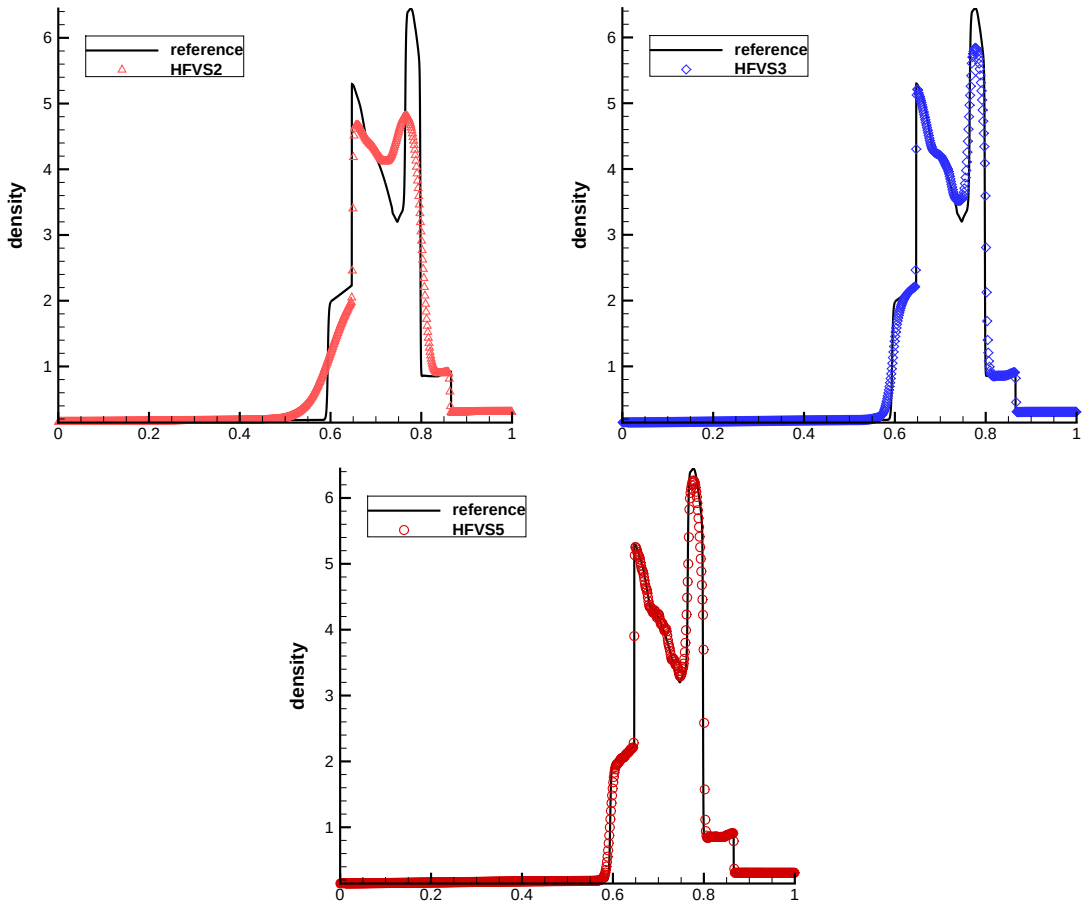

Figure 3: Example 3. density profiles for different schemes.

4.2.2 2D nonlinear problems

In this section, we present the numerical results of 2D Euler equations:

$$\frac{\partial \vec{W}}{\partial t} + \frac{\partial \vec{F}(\vec{W})}{\partial x} + \frac{\partial \vec{G}(\vec{W})}{\partial x} = 0$$

where

$$\vec{W} = (\rho, \rho U, \rho V, \rho E)^T$$

$$\vec{F}(\vec{W}) = \left(\rho U, \rho U^2 + P, \rho UV, \rho EU + PU\right)^T$$
$$\vec{G}(\vec{W}) = \left(\rho V, \rho UV, \rho V^2 + P, \rho EV + PV\right)^T$$

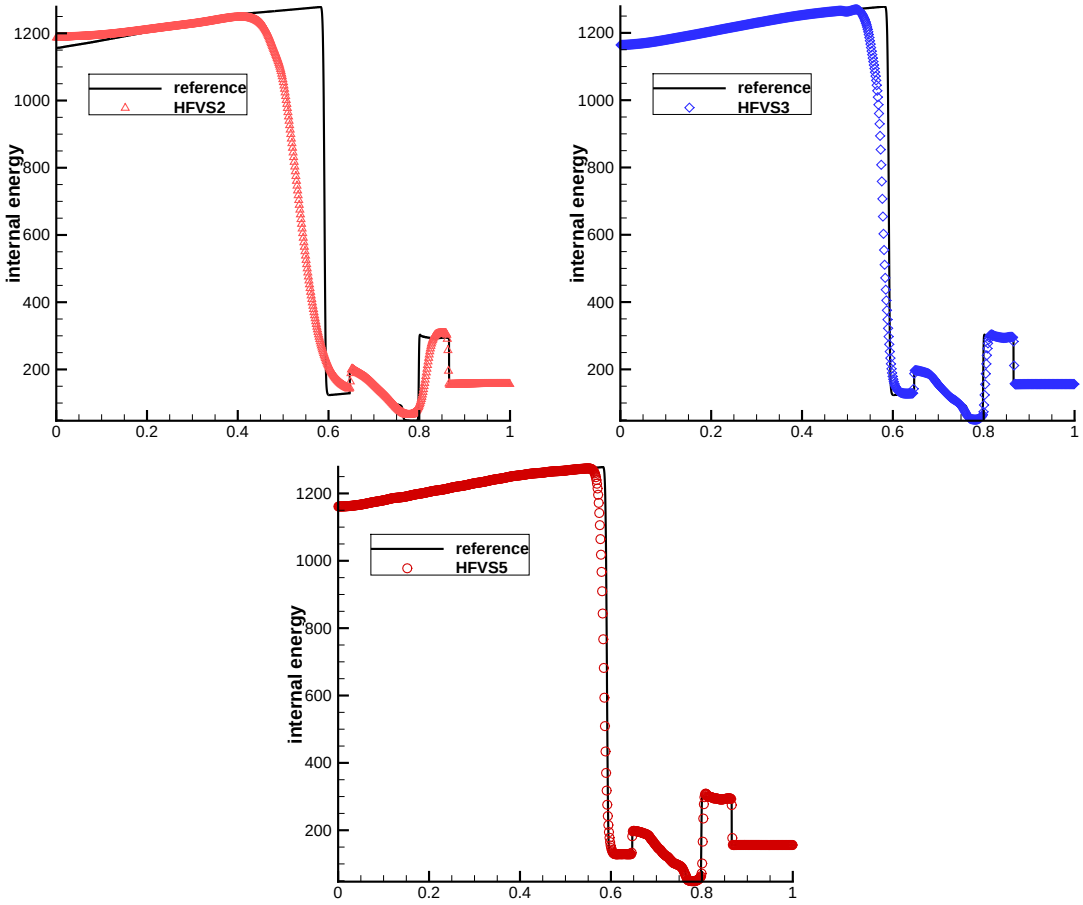

Figure 4: Example 3. internal energy profiles for different schemes.

and the equations of state is

$$P = (\gamma - 1)\,\rho\left(E - \frac{1}{2}U^2 - \frac{1}{2}V^2\right)$$

In the following case , $\gamma = 1.4$.

In this section, all numerical schemes use an optimal CFL number of 0.45.

Example 4. 2D Riemann problem. We want to show two cases which are simple extensions of 1D Riemann problems.

The first case sets computational domain as $[0,1]\times[0,1]$. And the boundary conditions are all outflow condition. The initial condition is given as

$$(\rho, U, V, P) = \begin{cases} (1.0, 0.0, 0.0, 1.0)\ , & x < 0.5 \ and \ y < 0.5 \\ (0.1, 0.0, 0.0, 0.1)\ , & x < 0.5 \ and \ y > 0.5 \\ (1.0, 0.0, 0.0, 1.0), & x > 0.5 \ and \ y > 0.5 \\ (0.1, 0.0, 0.0, 0.1), & x > 0.5 \ and \ y < 0.5 \end{cases}$$

We continue to compare the numerical results of HFVS with different order accuracy. The numerical results using the computational cells of 100×100 at $t = 0.15$ are presented. Fig.7 shows the density contours between the range of 0.1 and 1.0. We can draw the same conclusions as 1D case, i.e., all schemes can work well and HFVS can improve the accuracy and resolution if we increase the order of accuracy.

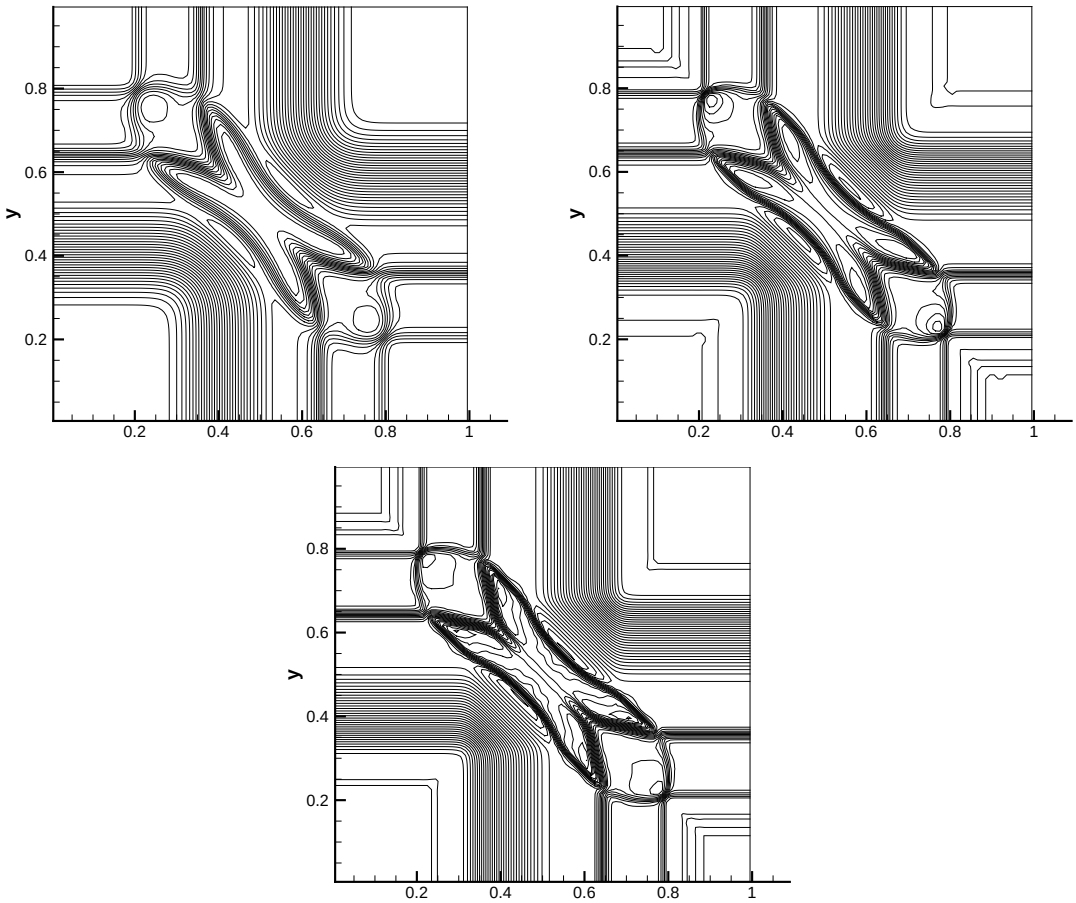

Figure 5: Example 4. density contours for different schemes,from left to right: HFVS2, HFVS3, HFVS5. 50 contours were fit between a range of 0.1 to 1.0.

The second case is a long time test. The computational domain is $[0, 1] \times [0, 1]$. And the boundary conditions are all reflective conditions. The initial condition is given as

$$(\rho, U, V, P) = \begin{cases} (1, 0, 0, 1), \sqrt{(x-0.5)^2 + (y-0.5)^2} \leq 0.3 \\ (0.125, 0, 0, 0.1), else \end{cases}$$

The numerical results using the computational cells of 100×100 at $t = 1.0$ are presented. Fig.7 shows the density contours between the range of 0.1 and 0.6. We

can draw the same conclusions as previous one, i.e., second order scheme gives a over-diffusion picture, third order scheme improve the accuracy, and fifth order scheme can give a sharp profile. It also demonstrates the efficiency of high order schemes.

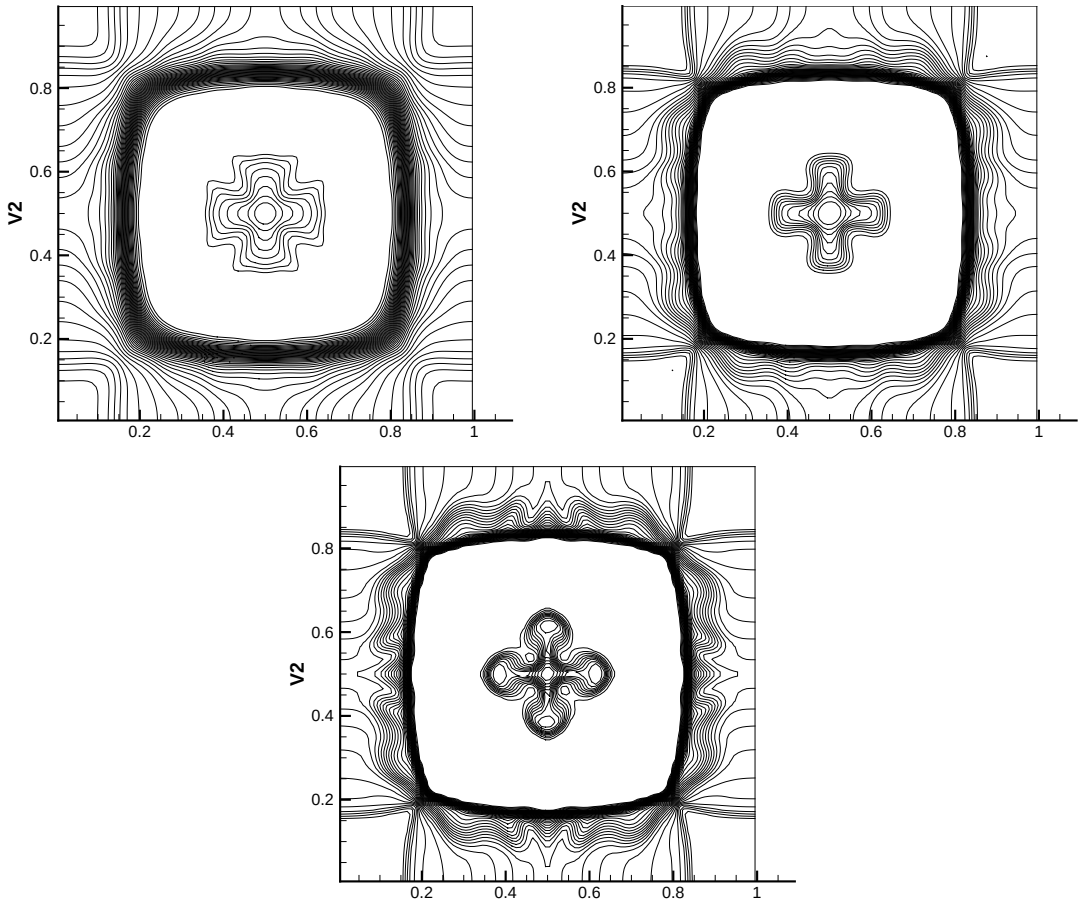

Figure 6: Example 4. density contours for different schemes,from left to right: HFVS2, HFVS3, HFVS5. 50 contours were fit between a range of 0.1 to 1.0.

4.3 Further discussions

4.3.1 The effective of different leading terms

As mentioned before, it seems possible to use different leading terms to couple with the same high derivative terms in HFVS. We compare three problem solver: Steger-Warming , HLLC and BGK, which represent FVS, Godunov and GKS approaches. Fig.7 shows second order results and Fig.8 shows fifth order results of Shu-Osher problem. We can observe that all schemes using different leading terms can work well. And

there are small differences among these scheme in low order case , while these differences almost vanish in high order case.

These numerical results do really demonstrate the possibility: the high order derivatives terms of HFVS can be used as a building block to couple with any Riemann problem solvers.

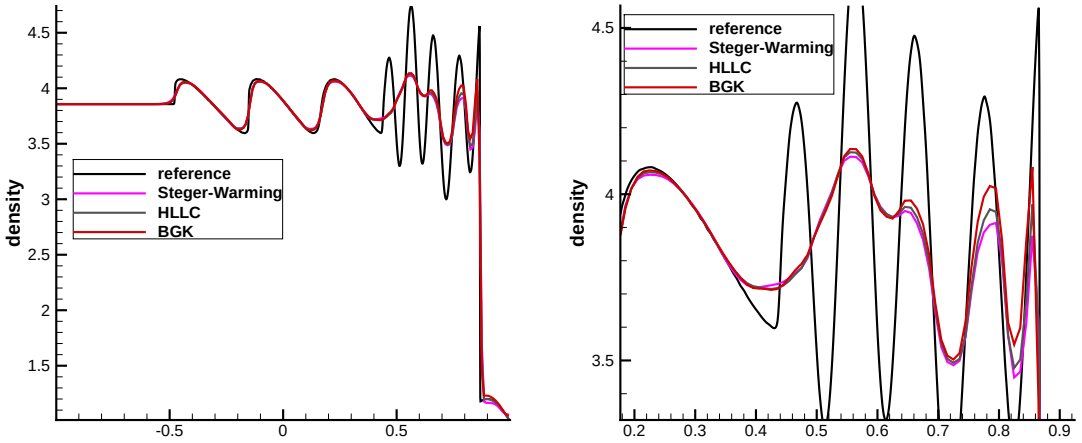

Figure 7: Shu-Osher problem. density profiles for HFVS2 using different leading terms.left : global picture, right: local enlargement.

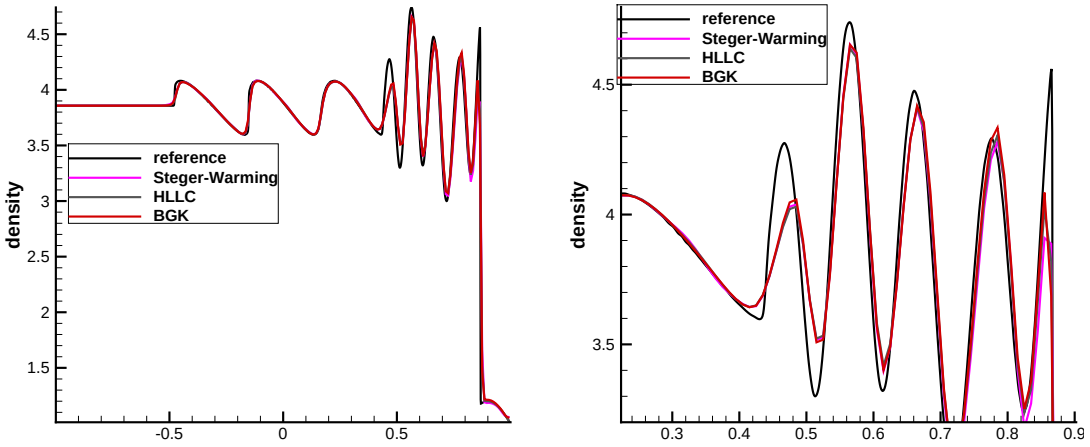

Figure 8: Shu-Osher problem. density profiles for HFVS5 using different leading terms. left : global picture, right: local enlargement.

4.3.2 Comparison between WENO and HFVS

In fact, the detailed comparison between WENO coupling with Runge- Kutta method with ADER can be found in [15]. It clearly show the advantages of ADER scheme.

Similarly, to demonstrate the efficiency of HFVS, we present the numerical results computed by WENO schemes coupling with Runge-Kutta methods. We should point out that we use the same reconstruction step in both WENO and HFVS.

Here, WENO3 and WENO5 represent third order and fifth order WENO schemes , and RK3 is third order Runge-Kutta method.

Table 2 shows the errors and accuracy of WENO3+RK3 and WENO5+RK3 using the same computational condition as Table 1. It is clearly, although WENO5+RK3 can get better accuracy than WENo3+RK3 , it can also achieve third order accuracy.

Fig.9 show the numerical results of Shu-Osher problems, which are computed by WENO and HFVS. The pictures show HFVS get better accuracy than WENO, no matter in case of third order or fifth order. This conclusion is similar to ADER and HGKS.

Table 3 show the computational cost of WENO and HFVS. We can also observe that HFVS almost use half CPU time of WENO. The reason is also clear: In every computational time step, HFVS use only one reconstruction step, while WENO should use three reconstruction steps. Although HFVS should calculate the high order terms, it is cheaper than reconstruction step.

Table 2: Errors and accuracy for WENO

METHOD	N	$L_1 ERROR$	ORDER	$L_2 ERROR$	ORDER	$L_\infty ERROR$	ORDER
WENO3+RK3	20	7.07E-01		7.07E-01		9.07E-01	
	40	5.25E-01	0.429	5.69E-01	0.313	7.54E-01	0.266
	80	1.26E-01	2.058	1.39E-01	2.033	1.94E-01	1.958
	160	1.77E-02	2.831	1.96E-02	2.826	2.76E-02	2.813
	320	2.24E-03	2.982	2.49E-03	2.976	3.52E-03	2.971
	640	2.81E-04	2.994	3.13E-04	2.991	4.42E-04	2.993
WENO5+RK3	20	7.04E-01		7.04E-01		7.07E-01	
	40	3.00E-01	1.230	3.40E-01	1.050	4.78E-01	0.564
	80	4.42E-02	2.762	4.92E-02	2.788	6.94E-02	2.784
	160	5.47E-03	3.014	6.07E-03	3.018	8.57E-03	3.017
	320	6.78E-04	3.012	7.53E-04	3.010	1.06E-03	3.015
	640	8.45E-05	3.004	9.39E-05	3.003	1.33E-04	2.994

Table 3: CPU time for WENO and HFVS

Method	Steps	Cpu time	Ratio
WENO3+RK3	1341	0.42	1
WENO5+RK3	1341	0.8268	1.96
HFVS3	1341	0.218	0.519
HFVS5	1341	0.374	0.89

5 Conclusions

In this paper, based on the idea of flux vector splitting scheme , we proposed a new scheme of arbitrary high order accuracy in both space and time to solve linear and nonlinear hyperbolic conservative laws. We start from splitting all the space and time derivatives in the Taylor expansion of the numerical flux into two parts: one part with positive eigenvalues, another part with negative eigenvalues. Then all the time derivatives can be replaced by space derivatives, according to a Lax-Wendroff procedure. A state-of-art WENO reconstruction polynomial is used to calculate the space derivatives . The new scheme is easy to implement, which will be very attractive for large CFD software.

In addition, there is an interesting result: the procedure of calculating high order terms of numerical flux can be used as a building block to extend the current first order schemes to very high order accuracy in both space and time.

Numerous numerical tests for linear and nonlinear hyperbolic conservative laws are presented to demonstrate that new scheme is robust and can be high order accuracy in both space and time.

References

[1] D.S.Balsara and C-W.Shu, Monotonicity preserving weighted essentially nonoscillatory schemes with increasingly high order of accuracy.J. Comp. Phys., 2000, v160, 405-452

[2] M.Ben-Artzi and J.Falcovitz. . A second-order Godunov-type scheme for compressible fluid dynamics. J. Comp. Phys. ,1984,55: 1C32.

[3] J.C.Butcher, Coefficients for the study of Runge-Kutta integration processes, J. Austral. Math. Soc. 3 (1963), 185C201.

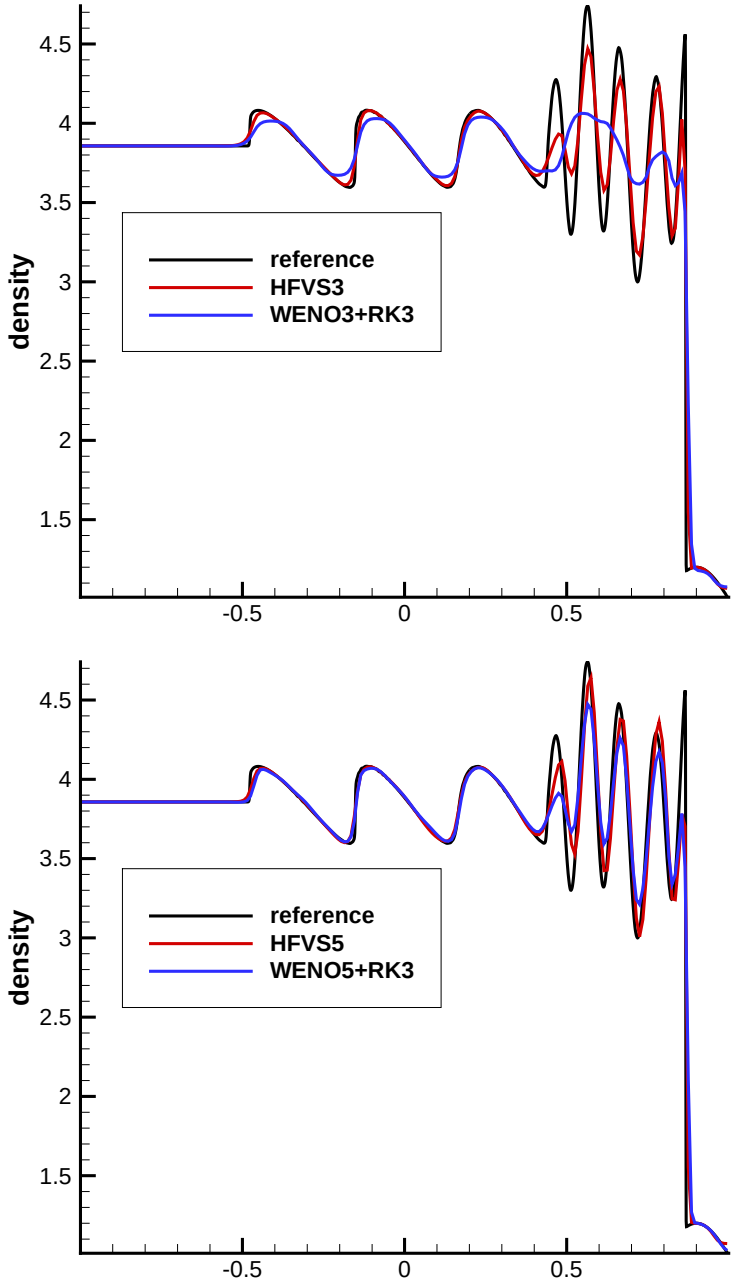

Figure 9: Shu-Osher problem. Density profiles of WENO and HFVS, left: third order schemes, right : fifth order schemes.

[4] Y.B.Chen , S.Jiang. Modified kinetic flux vector splitting schemes for compressible flows , J. Comp. Phys. , 2009, 228(10):3582C3604

[5] Y.B.Chen , S.Jiang. A non-oscillatory kinetic scheme for multi-component flows with the equation of state for a stiffened gas ,J. Comp. Phys., 2011 , 6:661C683

[6] A.Harten,B.Engquist,S.Osher and S.R.Chakravarthy, Uniformly high oder accuracy essentially non-oscillatory schemes III, J. Comp. Phys.. 1987,71,231-303

[7] A. Harten. On a class of high resolution total-variational-stable finite-difference schemes (with appendix by Peter D. Lax). SIAM J. Numer. Anal., 1984 21:123, .

[8] G.S.Jiang and C.W.Shu . Efficient implementation of weighed ENO schemes. J. Comput. Phys.,1996,126: 202C212.

[9] Q.Li, K.Xu, S.Fu. A high-order gas-kinetic NavierC Stokes solver. J. Comput. Phys., 2010, 229: 6715-6731

[10] N.Liu and H.Zh.Tang. A high-order accurate gas-kinetic scheme for one- and two-dimensional flow simulation. Commun. Comput. Phys., 2014,15:911-943.

[11] J.Luo, K.Xu. A high-order multidimensional gas-kinetic scheme for hydrodynamic equations , SCIENCE CHINA Technological Sciences, 2013, Vol56,No.10: 2370C2384

[12] P.L. Roe. Approximate riemann solver, parameter vectors and difference schemes. J. Comput. Phys., 1981,43:357C372

[13] C.W.Shu, S.Osher, Efficient implementation of essentially non-oscillatory shock-capturing schemes, ii, J. Comput. Phys., 1989,83:32C78.

[14] J.L. Steger and R. Warming,Flux vector splitting of the inviscid gas dynamic equation with application to finite differencemethods, J Compt. Phys, 1981,40: 263- 293.

[15] V.A.Titarev and E.F.Toro, Arbitrary high order Godunov approach, Journal of Scientific Computing, Vol. 17. No.1-4, December 2002

[16] E.F.Toro, M.Spruce and W.Speares. Restoration of the contact surface in the Harten-Lax-van Leer Riemann solver. Shock Waves. Vol. 4, pages 25-34, 1994.

[17] E.F.Toro and V.A.Titarev, TVD fluxes for the high-order ADER schemes, Journal of Scientific Computing, Vol. 24. No.3, September 2005

[18] B. van Leer. Towards the ultimate conservative difference scheme. IV: A new approach to numerical convection. J. comput. Phys., 23:276C299, 1977.

[19] Woodward and P.Colella. The numerical simulation of two-dimensional fluid flow with strong shocks. J. Comput. Phys., 54:115C173, 1984.